Spin-Cooling of the Motion of a Trapped Diamond

Tom Delord, P. Huillery, L. Nicolas, G. Hétet

Spin-Cooling of the Motion of a Trapped Diamond

T. Delord*,[1] P. Huillery*,[1] L. Nicolas,[1] and G. Hétet[1]

[1] *Laboratoire de Physique de l'Ecole normale supérieure, ENS, Université PSL, CNRS, Sorbonne Université, Université Paris-Diderot, Sorbonne Paris Cité, Paris, France.*

Observing and controlling macroscopic quantum systems has long been a driving force in research on quantum physics. In this endeavor, strong coupling between individual quantum systems and mechanical oscillators is being actively pursued [1–3]. While both read-out of mechanical motion using coherent control of spin systems [4–9] and single spin read-out using pristine oscillators have been demonstrated [10, 11], temperature control of the motion of a macroscopic object using long-lived electronic spins has not been reported. Here, we observe both a spin-dependent torque and spin-cooling of the motion of a trapped microdiamond. Using a combination of microwave and laser excitation enables the spin of nitrogen-vacancy centers to act on the diamond orientation and to cool the diamond libration *via* a dynamical back-action. Further, driving the system in the non-linear regime, we demonstrate bistability and self-sustained coherent oscillations stimulated by the spin-mechanical coupling, which offers prospects for spin-driven generation of non-classical states of motion. Such a levitating diamond operated as a compass with controlled dissipation has implications in high-precision torque sensing [12–14], emulation of the spin-boson problem [15] and probing of quantum phase transitions [16]. In the single spin limit [17] and employing ultra-pure nano-diamonds, it will allow quantum non-demolition read-out of the spin of nitrogen-vacancy centers under ambient conditions, deterministic entanglement between distant individual spins [18] and matter-wave interferometry [16, 19, 20].

Since the celebrated Einstein and de Haas' experiment in 1915 [21], much work has been carried out in the detection of atomic spins through mechanical motion [22], culminating in the observation of a magnetic force from single spins [10, 11] and magnetometry at the nanoscale [13]. Conversely, single spins and qubits have also been utilized to sense the motion of objects close to the quantum ground state. Single qubit thermometry of mechanical oscillators at the quantum level was realized using superconducting qubit coupled to membranes [4, 8] and nitrogen-vacancy (NV) centers coupled to cantilevers [5–7]. A crucial next step is to reach strong coupling between long-lived spins and mechanical oscillators, which will enable ground state cooling, as in tethered quantum opto-mechanical platforms [23–25], and the observation of quantum superpositions of macroscopic systems [2]. One further prospect is the entanglement between multiple spins [18], with far reaching implications in quantum information science and metrology [26]. Obtaining coupling rates that surpass both the decoherence of the spin and of the mechanical system is however still a challenge for most state-of-the-art platforms. Recently, there has been renewed focus on levitating objects [27, 28] motivated by the low mass and high Q-factors that they offer, together with the possibility to cool their motion using embedded spins [19]. There is a strong analogy between this platform where spins move a levitating crystal and laser-cooled atoms where electrons move atomic nuclei. It may thus be forecast that a levitating particle containing a few long-lived spins will ultimately reach similar level of control as trapped ions [3] with bright prospects for the aforementioned applications.

In this work, we report on a controllable torque induced by the spins of atoms embedded into a macro-object. Specifically, we couple the spin of many nitrogen-vacancy (NV) centers to the orientation of a trapped diamond particle. This coupling then enables us to show read-out of the NV centers spin resonance together with cooling and lasing of the diamond motion.

The crystallographic structure of NV centers is depicted in Fig. A-a). The spin-spin interaction between the two electrons in the NV center ground state lifts the degeneracy of the spin triplet eigenstates by $D = 2.87$ GHz at room temperature. Such an interaction implies that the NV center has a preferential quantization axis that is along one of the four crystal axes $\langle 111 \rangle$. In the presence of a magnetic field $\mathbf{B}$ at an angle ϕ with respect to the NV axis, the energy difference between the two energy eigenstates $|m'_s = \pm 1\rangle$ is about $\gamma_e B\phi$, where γ_e is the gyromagnetic ratio of the electron. Spin control can then be performed using optical and microwave excitation and the angular dependence of the NV spin energy eigenstates is expected to allow rotation and cooling of the diamond angular motion. Once in a magnetic state *via* a resonant microwave excitation, the NV center will tend to align the corresponding diamond crystalline axis to the magnetic field, as illustrated in Fig. A-a-i). Further, laser triggered relaxation from the excited state can then extract the work exchanged between the spin magnetic energy and the librational motion (see Fig. A-a-ii)).

In our experiment, harmonic librational (sometimes called torsional, pendular or rotational) confinement is provided both by the Paul trap and the particle asymmetry. We measure the diamond libration using the laser reflection off the diamond surface. The μm size roughness on our 15 μm particle enables a specular pattern to be detected at the particle image plane, which after mode-matching one of the many bright spots to an optical fiber yields an angular sensitivity of about 0.3 mrad/$\sqrt{\text{Hz}}$ and a resolution of about 10 mrad/Mcounts/s (see Methods). Under vacuum conditions (≈ 1 mbar), the signal power spectrum plotted in Fig. A-b) shows harmonic motion of the three librational modes with frequencies $\omega_\phi/2\pi$ ranging from 200 Hz to 1 kHz and with a damping rate of about 15 Hz. Fig. A-b) also shows an optically detected magnetic resonance (ODMR) spectrum for a diamond outside the trap, in the presence of a magnetic field $B \approx 30$ G. Eight transitions, corresponding to the projections of the B field onto the four NV orientations are observed, with typical spin decoherence rates $1/T_2^* \approx 7$ MHz.

We now measure the diamond rotation induced by the $N \approx 10^9$ NV electronic spins inside the diamond, with the same optical read-out as for the librational mode detection, as depicted in Fig. B-a)-i). The expected magnitude of the spin-torque is $\Gamma_s = \hbar N \gamma_e B S_z \approx 10^{-19}$N.m. Here S_z is the population in one of the magnetic states, determined by the competition between the microwave and laser polarization (both at rates in the 100 kHz range). This torque gives a displacement of the particle angle in the trap $\delta\phi = \Gamma_s / I\omega_\phi^2 \approx 10$ mrad, where $I \approx 10^{-22}$ kg.m^2 is the particle moment of inertia. As can be seen in Fig. B-a)-ii), sweeping a microwave around the spin resonances indeed enables conspicuous features to appear. Once in the magnetic state $|m'_s = -1\rangle$ or $|m'_s = +1\rangle$, the NV centers tend to align or anti-align the diamond orientation to the magnetic field, which is manifest in the anti-correlation between the detected intensity levels for all pairs of transitions. A standard ODMR is also measured under the same magnetic field amplitude and measurement time (see Fig. B-a)-iii)) demonstrating perfect correlation in the frequency of the peaks in the two measurements.

This spin-mechanical effect is in fact much richer than a static spin-dependent torque. As shown in Fig. A-a), the NV centers are magnetized through a microwave tone whose detuning from the NV resonances changes as the diamond rotates. To first order, such a torque will increase (resp. decrease) the confinement of the Paul trap if the microwave is blue (resp. red) detuned from the spin-resonance at the equilibrium angular position. Further, since the spin lifetime is on the order of the libration period, it enables dynamical back-action. A delay between the NV magnetization and the angular oscillation, observed in [29], indeed induces a torque that depends on the velocity,

in close analogy with opto-mechanical schemes [23–25] and with Sisyphus cooling of cold atoms. The net result is a pronounced cooling (resp. heating) of the diamond motion when the microwave is red (resp. blue) detuned from the spin resonance as sketched in Fig. B-b). In order to observe such spin-spring and spin-cooling effects, we monitor the librational power spectrum as a function of the microwave detuning from the electronic spin resonance. Fig. B-b) shows the result of measurements taken for three different microwave frequencies with a Rabi frequency of 10 kHz. A strongly modified spring and damping of the mechanical mode are observed. Assuming that the initial temperature is 300 K (see Methods), the resulting temperature after spin-cooling is here 80 K. Fig. B-c) shows measurements of the damping rate and spring effects as a function of microwave frequency in good agreement with a theoretical model (see Methods). Cooling is at present limited by heating from the microwave excitation of the motion on the blue side. This could be eliminated by increasing the trapping frequency $\omega_\phi/2\pi$ above the NV spin transition linewidth.

We now make a step into a regime where the spin-mechanical interaction induces non-linear effects on the librational mode. With a stronger spin-torque (see Methods), Fig. C-a)-i) displays the expected bistable behavior for the angular degree of freedom when the microwave is scanned across the spin resonance. The angle can be found at two metastable positions A or B depending on the history of the angular trajectory (see SI). The hysteresis behavior is indeed observed in the experiment, and shown in Fig. C-a)-ii). The evolution of the particle orientation over time at a fixed microwave tone is also plotted in Fig. C-a)-iii). Interestingly, the particle orientation jumps from site A to B in a seemingly unpredictable manner due to random kicks given to the particle. The average population at the angular position B can also be studied as a function of different microwave detunings and increases as the microwave is tuned towards resonance (see extended data and SI).

Let us now set the microwave frequency to the blue side of the spin-resonance in this strong spin-torque regime. Fig. C-b)-i) shows the power spectral density as a function of the microwave pump power, where a transition from Brownian motion to a self-sustained oscillation is observed. Such a lasing-like action of a mechanical oscillator was observed in the first radiation pressure cooling experiments [6] with proposed applications in metrology. The spin-mechanical gain that enables such lasing action here is provided by blue detuned microwave excitation which amplifies the angular motion up to a point where losses are compensated by the magnetic gain. The oscillator energy as a function of the microwave power is shown in Fig. C-b)-ii). Lasing threshold is observed at 6 mW of microwave excitation. Another signature of mechanical lasing is shown in Fig. C-b)-iii), which displays the probability distribution (PD) of the angular degree of freedom with and without microwave. Under blue detuned microwave excitation, the probability distribution departs from the Gaussian process (red curve) for Brownian motion, and turns to the characteristic PD of a coherent oscillation (blue curve). This effect shows that the librational mode can operate stably, deep in the non-linear regime and highlights further the analogy between the present spin-mechanical platform and opto-mechanical systems.

Coupling individual spins to the motion of a macroscopic oscillator will have far reaching applications in fundamental science, quantum information and metrology. The present spin-dependent torque itself may be employed for detecting atomic defects with electrons spins that cannot be efficiently detected through ODMR. Further, the approach may also be applied to other torsional nano-mechanical platforms [29, 30], which can exploit the long NV spin-lattice relaxation at low temperatures for longer interrogation times and efficient cooling. Last, operating in the sideband resolved regime where $\omega_\phi/2\pi \gg 1/T_2^*$ can be realized after modest improvements to the present set-up. We estimated that using a 1 μm diameter pure diamond grown by chemical vapor deposition (CVD) attached to a 1 μm diameter ferromagnet, would enable entering the sideband resolved regime for this hybrid structure. Librational frequencies $\omega_\phi/2\pi$ above 200 kHz have indeed been observed recently [29] and NV centers with $1/T_2^* = 50$ kHz electron-spin decoherence rates can readily be obtained in CVD grown microdiamonds enriched in ^{12}C. Entering this regime would offer immediate prospects for ground state cooling the diamond libration and for multipartite spin-entanglement and would provide strong impetus to bridge the gap between trapped particles and trapped atoms.

[1] P. Treutlein, C. Genes, K. Hammerer, M. Poggio, and P. Rabl, "Hybrid mechanical systems," in *Cavity Optomechanics: Nano- and Micromechanical Resonators Interacting with Light*, edited by M. Aspelmeyer, T. J. Kippenberg, and F. Marquardt (Springer Berlin Heidelberg, Berlin, Heidelberg, 2014) pp. 327–351.

[2] P. Rabl, P. Cappellaro, M. V. G. Dutt, L. Jiang, J. R. Maze, and M. D. Lukin, Phys. Rev. B **79**, 041302 (2009).

[3] D. Leibfried, R. Blatt, C. Monroe, and D. Wineland, Rev. Mod. Phys. **75**, 281 (2003).

[4] M. D. LaHaye, J. Suh, P. M. Echternach, K. C. Schwab, and M. L. Roukes, Nature **459**, 960 EP (2009).

[5] S. Kolkowitz, A. C. Bleszynski Jayich, Q. P. Unterreithmeier, S. D. Bennett, P. Rabl, J. G. E. Harris, and M. D. Lukin, Science **335**, 1603 (2012).

[6] O. Arcizet, V. Jacques, A. Siria, P. Poncharal, P. Vincent, and S. Seidelin, Nat Phys **7**, 879 (2011).

[7] D. Lee, K. W. Lee, J. V. Cady, P. Ovartchaiyapong, and A. C. B. Jayich, Journal of Optics **19**, 033001 (2017).
[8] A. D. O'Connell, M. Hofheinz, M. Ansmann, R. C. Bialczak, M. Lenander, E. Lucero, M. Neeley, D. Sank, H. Wang, M. Weides, J. Wenner, J. M. Martinis, and A. N. Cleland, Nature **464**, 697 EP (2010).
[9] P. Treutlein, D. Hunger, S. Camerer, T. W. Hänsch, and J. Reichel, Phys. Rev. Lett. **99**, 140403 (2007).
[10] M. J., PoggioM., D. L., and RugarD., Nat Nano **2**, 301 (2007).
[11] D. Rugar, R. Budakian, H. J. Mamin, and B. W. Chui, Nature **430**, 329 EP (2004).
[12] P. H. Kim, B. D. Hauer, C. Doolin, F. Souris, and J. P. Davis, Nature Communications **7**, 13165 EP (2016).
[13] J. A. J. Burgess, A. E. Fraser, F. F. Sani, D. Vick, B. D. Hauer, J. P. Davis, and M. R. Freeman, Science **339**, 1051 (2013).
[14] T. M. Hoang, Y. Ma, J. Ahn, J. Bang, F. Robicheaux, Z.-Q. Yin, and T. Li, Phys. Rev. Lett. **117**, 123604 (2016).
[15] A. J. Leggett, S. Chakravarty, A. T. Dorsey, M. P. A. Fisher, A. Garg, and W. Zwerger, Rev. Mod. Phys. **59**, 1 (1987).
[16] Z. Yin, N. Zhao, and T. Li, Science China Physics, Mechanics & Astronomy **58**, 1 (2015).
[17] G. P. Conangla, A. W. Schell, R. A. Rica, and R. Quidant, Nano Letters **18**, 3956 (2018).
[18] P. Rabl, S. J. Kolkowitz, F. H. L. Koppens, J. G. E. Harris, P. Zoller, and M. D. Lukin, Nature Physics **6**, 602 EP (2010).
[19] Z.-q. Yin, T. Li, X. Zhang, and L. M. Duan, Phys. Rev. A **88**, 033614 (2013).
[20] M. Scala, M. S. Kim, G. W. Morley, P. F. Barker, and S. Bose, Phys. Rev. Lett. **111**, 180403 (2013).
[21] A. Einstein and W. J. de Haas, "Experimenteller Nachweis der Ampèreschen Molekularströme," Deutsche Physikalische Gesellschaft **17** (1915).
[22] G. Alzetta, E. Arimondo, and C. Ascoli, Nuovo Cimento B **52:292** (1967).
[23] O. Arcizet, P. F. Cohadon, T. Briant, M. Pinard, and A. Heidmann, Nature **444**, 71 EP (2006).
[24] S. Gigan, H. R. Böhm, M. Paternostro, F. Blaser, G. Langer, J. B. Hertzberg, K. C. Schwab, D. Bäuerle, M. Aspelmeyer, and A. Zeilinger, Nature **444**, 67 EP (2006).
[25] A. Schliesser, R. Rivière, G. Anetsberger, O. Arcizet, and T. J. Kippenberg, Nature Physics **4**, 415 EP (2008).
[26] M. S. J. Barson, P. Peddibhotla, P. Ovartchaiyapong, K. Ganesan, R. L. Taylor, *et al.*, Nano Letters **17**, 1496 (2017).
[27] D. E. Chang, C. A. Regal, S. B. Papp, D. J. Wilson, J. Ye, O. Painter, H. J. Kimble, and P. Zoller, Proceedings of the National Academy of Sciences **107**, 1005 (2010).
[28] O. Romero-Isart, M. L. Juan, R. Quidant, and J. I. Cirac, New Journal of Physics **12**, 033015 (2010).
[29] P. Huillery, T. Delord, L. Nicolas, M. Van Den Bossche, M. Perdriat, and G. Hétet, arXiv e-prints , arXiv:1903.09699 (2019), arXiv:1903.09699 [quant-ph].
[30] M. Wu, N. L. Y. Wu, T. Firdous, F. Fani Sani, J. E. Losby, M. R. Freeman, and P. E. Barclay, Nature Nanotechnology **12**, 127 EP (2016).

Acknowledgments We would like to thank R. Blatt, C. Voisin, Y. Chassagneux, E. Baudin and S. Deléglise for discussions.

Author Contributions T. D. and P. H. contributed equally to this work. T. D, P. H., L. N. and G. H. performed the spin-torque experiments; T. D, P. H., and G. H. analyzed the data and performed the modeling with assistance from L. N., and G. H., T. D and P.H. wrote the manuscript. All authors contributed to the interpretation of the data and commented on the manuscript.

MAIN FIGURE LEGENDS

A. Figure 1

Spin and mechanical systems. a) Sketch of the diamond crystallographic structure hosting NV defects. i) Equilibrium position of the diamond in the Paul trap before the micro-wave excitation. The principal diamond axis $\vec{P}$ points towards the main trap axis. The ground state spin-levels and microwave drive are depicted below. The magnetic field $\vec{B}$ lifts the degeneracy between the excited spin states by about $\gamma_e B\phi$, where ϕ is the angle between the magnetic field and the NV axis. The microwave signal prepares the NV in a magnetic state, which induces a torque to the diamond. ii) Once at the new angular position, the spin projection onto the magnetic field is changed to $\gamma_e B\phi'$. The microwave is then no longer resonant : the spin relaxes to the ground state and the diamond returns to its initial position. b) Measurements of the three librational modes undergoing Brownian motion at 1 mbar of vacuum pressure (top) and of the typical electronic spin resonances from the NV ensemble within a microdiamond outside the trap using standard optically detected magnetic resonance (ODMR) at 30 G (below). Solid lines are a fit to the data.

B. Figure 2

Spin-dependent torque and cooling of a levitating diamond a) i) Sketch of the laser beam deflection induced by the NV spin-torque. ii) Detected APD count-rate $I_{\rm scatt}$ as a function of the microwave frequency. iii) corresponding ODMR. b) Cooling/heating cycle of the librational motion induced by the spin-mechanical coupling (left). Power spectrum of the reflected light intensity from the diamond surface when the microwave is tuned to the blue (trace i)), to the center (trace ii)), and to the red (trace iii)) of the spin resonance (on the right). The alignment of the reflected light from the diamond surface in the fiber was optimized to only let these two librational modes appear in the power spectrum. Note that the particle is here different from the one used in figure 1b. c) Damping rates and librational mode frequencies as a function of the microwave detuning. Plain lines show a fit to the experimental data using numerical simulations.

C. Figure 3

Non-linear spin-motion dynamics a) **Bistability** i) Evolution of the particle angle as a function of the microwave detuning. ii) Hysteresis behavior of the particle orientation when the microwave signal is scanned from the red to the blue (blue curve) or from the blue to the red (red curve), as indicated by the arrows. iii) Particle orientation as a function of time for a fixed microwave tuned to the red side of the spin transition, showing angular jumps between two stable sites A and B. b) **Phonon lasing** i) Evolution of the power spectrum of the librational motion as a function of the microwave power towards lasing. ii) Oscillator energy as a function of microwave intensity using microwave powers ranging from -44 up to -16 dBm in steps of 4 dBm. The dashed lines are a fit to the data. iii) Histogram of the Brownian and lasing angular motions.

Methods

Microdiamond properties The diamonds that we employ are in the form of a powder of particles that have a diameter of 15 μm. They are supplied by the company Adamas, which produces diamonds with a concentration of NV centers in the 3-4 ppm range, corresponding to 1.5 to 2×10^9 NV centers per microdiamond. Using the same collection optics as was used in [1] we could also estimate the number of optically addressed NV centers to lie in that same range. This is 4 to 5 orders of magnitude larger than the concentration compared to the experiments reported in [1–3], where no spin-torque was observed. Under continuous laser excitation at around 10 μW, the diamond starts to heat up at 0.1 mbar, at similar pressures than in [2] which points towards the role played by other impurities than the NV centers in the heating observed in [2]. The pressure we operate at is 1 bar for the spin-torque measurements shown in Figure 2 in the main text, and in the mbar range for the cooling and phonon-lasing experiments.

The Paul trap We operate with a Paul trap that is similar to the one used in [1] except that the particles are stably trapped at the bottleneck region of the trap, where both the electric field gradient and anisotropy are stronger, yielding higher librational confinement. Below 1 mbar, the diamond starts to rotate due to a locking mechanism induced by the Paul trap drive, making it impossible to observe the spin-dependent torque, which relies on very stable libration.

NV spin polarization and read-out Due to an intersystem crossing in the excited state of the NV centers, the electronic ground state $|0\rangle$ is brighter then the ground state $|1\rangle$ upon green laser optical illumination. This provides a means to read out the Zeeman splitting by scanning a microwave tone around the resonance, carrying out Optically Detected Magnetic Resonance (ODMR). Here, the microwave is applied directly on the trapping electrode, which provides an efficient means to excite the spins. The photoluminescence is detected using standard confocal microscopy. We use about 100 μW of laser light at 532 nm to polarize the NV centers. The laser is focussed via a lens inside the vacuum chamber which has a numerical aperture of 0.5 and a working distance of 8 mm. The focal point of the laser is kept few tens of micrometer away from the microdiamond to mitigate the effect of radiation pressure and to enable laser excitation of the whole diamond [1, 3]. To measure polarization rate to the ground and to the excited magnetic states, we carry out the sequence depicted in Fig. H-a). The photo-luminescence (PL) rate is measured as a function of the time τ for both sequences and is plotted in Fig. H-b). The laser induced polarization rate to the $m_s' = 0$ state is 3.3 kHz. The microwave polarization rate $\Gamma_M = \Omega^2 T_2^*$ (see SI) to the magnetic state $m_s' = -1$ is found to be 8 kHz when using -5 dBm of microwave power measured before a 25 dBm amplifying stage. An estimation based on both the ODMR width and a Ramsey sequence yields $T_2^* = 70$ ns, implying $\Omega/2\pi = 60$ kHz.

The exact degree of spin polarization cannot be estimated precisely without using a full numerical model and the 8 rate equations including mixing by the magnetic field transverse component. The magnetic field transverse component reduces the polarization time due to mixing of electron spin states both in the ground and excited levels. This enhances the probability of non-radiative crossing to the metastable level and reduces the ODMR contrast by 30%[4]. Overall, this reduces the degree of optical polarization to the $m_s' = 0$ spin state to about 60 %.

Detection and analysis of the librational modes The diamond motion is detected by collecting the back reflected green light from the diamond interface, separated from the excitation light using a polarizing beam splitter. The best sensitivity is achieved by taking advantage of the speckle pattern produced by the rough surface of the microdiamond under coherent illumination. At the particle image plane, which is located a few tens of centimeters away from the particle, an image is formed with an additional speckle feature. To detect the diamond motion, we focus a small area of this image onto a single-mode optical fibre and detect the photons transmitted through the fibre with a single-photon avalanche photodiode. The detected signal is then highly sensitive to the particle position and orientation.

Angular displacement sensitivity For a given levitating particle, we can optimize, in real time, the signal coming from the angular displacement of the particle by selecting the most favorable region of the particle image. To do this, we look at our optical signal while switching a microwave field tuned to one ODMR transition at a frequency of 1 Hz. Alignment is done by maximizing the change in the coupled light intensity as the diamond jumps between two angular positions. The linearity of the coupled light with the rotating angles can finally be assessed by looking at higher order of the harmonic motion once the librations frequencies are identified.

While being a sensitive measurement of the angular displacement, our optical signal is not an absolute measurement. The spin-torque vector $\vec{\Gamma_s}$ is orthogonal to the plane defined by the magnetic field and the NV axis (it tends to align the NV axis to the B field). However, because the angular confinement is not isotropic, the particle rotation angle is not necessarily collinear to the spin-torque. Determining the exact three-dimensional rotational dynamics of the particle would necessitate knowledge about the orientation of the NV axes with respect to the principal axes of the angular motion.

Using NV magnetometry, the mechanically detected spin resonance can nonetheless be used to relate the optical signal change to the angular displacement of the particle. A set of three mechanically detected spin resonances

corresponding to three different microwave powers are shown in Fig. G-a) of the extended data, under a magnetic field of 144 G. The minima of each curve fall on the dashed line. The lower panel of Fig. G-a) is a theoretical curve where the angle between the NV axis and the magnetic field direction is plotted as a function of the frequency of the NV spin transition. This curve is obtained by diagonalizing the NV spin Hamiltonian in the presence of a magnetic field of 144 G. Since the maximum magnetization of the NV spins is obtained when the microwave field is resonant with the spin transition, one can relate the maximal change in the optical signal (ΔS) to the variation of the angle between the NV axis and the magnetic field direction ($\Delta\theta_{NV}$). Doing so, we obtain here a resolution of 43 mrad/Mcounts/s. Fig. G-b) shows a time trace of the optical signal upon brownian motion of the particle. From the standard deviation of this signal and the above calibration, we obtain an angular displacement sensitivity of 0.3 mrad/$\sqrt{\text{Hz}}$.

These numbers are however only upper bounds for our resolution and sensitivity. To explain why this is the case, Fig. G-c) shows a sketch of the angular motion of the diamond after magnetizing one class of NV spins. For simplicity, we consider rotation about two axes here. In a referential frame with axes given by the principal librational mode directions, we can parametrize the orientation of the NV axis in a subspace defined by the two angular coordinates θ_x and θ_y. The orientation without magnetization ($M_z = 0$) is given by the trap and particle geometry and labelled O. The point B in this space is the direction of the magnetic field. Upon magnetization, a torque is applied to the particle such that the orientation follows the OB trajectory over time. However due to different confinement of the librational modes ω_x and ω_y along the x and y axes, the angular motion takes place along a different trajectory.

In our experiments, the orientation of the magnetic field and NV axes relative to the principal axis of the libration is unknown. This prevents us from fully calibrating our detected angular motion. Nevertheless, provided that the detection is optimized to the librational mode having the highest confinement, we can ensure that the detected angular displacement θ_d is smaller than the angular displacement θ_{NV} sensed by the NV spins. This can be seen in Fig. G-c), where we note NV the equilibrium position when $\omega_x > \omega_y$. Our calibration method thus gives an upper bound to the obtained resolution and sensitivity. The optimization of the detection is performed by monitoring the power spectrum and tuning the speckle angle at the entrance of the fiber to maximize the power spectrum of the mode with the largest frequency. Fig. G-d) shows the power spectrum of the brownian motion for two detection alignments. In red, all three librational modes, indicated with the black arrows, are clearly visible. In blue, the detection is tuned to be mainly sensitive to the mode with the highest confinement frequency. The latter detection tuning is used for the data shown in a) and b).

The sensitivity could be improved by collecting all the speckle pattern using a SPAD camera rather than just a fraction of it as we do now. Using a shorter laser wavelength would also straightforwardly improve the sensitivity. Another technical limitation comes from the trapped diamond motion in other modes than the libration mode of interest which adds noise to the angular displacement signal. In this regard, active stabilization of the center of mass will greatly increase the sensitivity.

Power Spectral density Using the above described detection method, motional frequencies can be observed by sending the detected signal to a spectrum analyzer. Under vacuum (1 mbar), the power spectral exhibits narrow peaks at the trapping frequencies of the motional modes which are driven by the Brownian motion (see Fig 1-b) in the main text). For each librational mode, the power spectrum is fitted by the formula obtained in the SI :

$$S_\phi(\omega) = \frac{2\gamma kT}{I((\omega_\phi^2 - \omega^2)^2 + \gamma^2\omega^2)}. \tag{1}$$

The librational modes can in fact be unambiguously identified (and separated from the center of mass modes) using the NV centers induced torque. By switching on and off a microwave field tuned to one spin resonance at the same period as that of one diamond libration, one performs parametric excitation of that librational mode. In our experiments, a sequence of five microwave pulses is enough to displace the angle above the Brownian thermal noise. Following a parametric excitation sequence, the diamond orientation "ring-down", or decay, is observed. A typical decay curve is shown in Fig. 4-a). We typically find librational frequencies in the 100 Hz to 1 kHz range.

Parameters used for the spin-dependent torque measurements The ODMR and spin-mechanical measurement scans shown in Fig 2-a) of the main text are taken under atmospheric pressure. The green laser power was 330 μW and the microwave power set to 0 dBm. The magnetic field is around 95 G. For the mechanically detected spin resonance of trace ii), the microwave detuning is scanned in 2 MHz steps with a duration of 10 ms per points. During those 10ms, the diamond orientation has enough time to reach its equilibrium position and the spin torque effect can be observed. The average count-rate is 2.3×10^6 s^{-1} for a total averaging time of 10 minutes. For the ODMR trace iii), the microwave detuning is scanned by step of 2 MHz with a duration of 1ms per points. For each point, the microwave field is switched off for the first 0.5ms and switched on for the last 0.5 ms during which the signal is acquired. This prevents mechanical effects from altering the detected NV centers photo-luminescence (PL) signal. The PL count rate is 5×10^6 s^{-1} and the total averaging time for this measurement was 3h.

Estimation of the temperature Measurement of the temperature associated with the librational modes can only be an estimate. Obtaining a precise temperature value would require knowledge about the moment of inertia of the particle, which is prone to strong systematic errors. The standard method is to vary the pressure [5] while observing the power spectrum : over the pressure range where its area is constant (to satisfy Liouville's theorem under adiabatic transformation) the librational mode temperature is known to be 300 K as it is thermalized with the gas temperature. In our case, pressure variations slightly change the orientation and position of the trapped particle and, incidentally, the sensitivity to angular motion. This prevents such method from being used. However several measurements support the fact that the external degrees of freedom of the particle are thermalized at 300 K when operating in the mbar pressure range. First, we measured the particle internal temperature with our typical laser powers *via* NV thermometry [2] and found it to be close to 300 K. This insures that no heating of the libration modes comes from the heating of the gas surrounding the particle [6]. We observed that heating of the particle by the laser starts below 0.1 mbars, similar to what was measured using diamonds that were doped with a three orders of magnitude smaller NV concentration. Several sources of noise could also heat up the particle, such as the laser induced torque [3] or charge fluctuations. Heating by the former can be excluded as no noticeable changes of the power spectrum shape occur when laser power is increased up to 1 mW.

Parameters and calibration used for the cooling measurements The power spectrum of the detected librational modes depends strongly on the particle angle. For the same motional amplitude, a change in the particle angle potentially implies a different speckle pattern, which in turn changes the power spectrum sensitivity. Since the particle angle changes with the microwave detuning and power, different power spectra cannot be directly compared when the parameters are changed. The three traces i), ii) and iii) in Fig. 2-b) in the main text have thus been obtained at the same particle angle to enable quantitative comparison between their areas. Operating at the same particle angle was ensured by performing a resonant spin-mechanical detection at different microwave amplitudes and choosing pairs of microwave frequencies and powers that correspond to the same count rates. As shown in the data in Fig. 4-b), we chose microwave detunings corresponding to the points 1-2-3 for the two traces i) and ii) taken at microwave powers of -20 dBm and -10 dBm respectively. The frequencies, which are 2.617, 2.623 and 2.634 GHz, respectively to the blue, resonant and red side of the spin resonance all correspond to the same angle under these power conditions. A fit to the experimental curves in Fig. 2-b) was obtained using the formula

$$S_\phi(\omega) = \frac{2\gamma_{\text{eff}} kT}{I((\omega_{\text{eff}}^2 - \omega^2)^2 + \gamma_{\text{eff}}^2 \omega^2)}. \tag{2}$$

The dependence of the damping γ_{eff} and frequency shift ω_{eff} with the microwave detuning shown in Fig. 2-c) was obtained using parametric excitation of the librational mode at 480 Hz. The microwave power is -10dBm and for this measurement, the above mentioned calibration issue (change in the sensitivity when the microwave detuning is varied) is not relevant. In order to extract the damping and shifts, the resulting ring-down was fitted by the formula

$$\begin{aligned} S(t) = {} & A_1 \sin(\omega_{\text{eff}} t + \phi) \exp(-\gamma_{\text{eff}} t/2) \\ & + A_2 \sin(\omega_2 t + \phi_2) \exp(-\gamma_2 t/2) + A_0, \end{aligned} \tag{3}$$

where the second exponentially damped sinus takes into account the slightly excited librational mode at 590 Hz. Three of these ring-down traces are shown in the Fig. 4-c). For each curve, the averaging time is around 100 s. An estimation of the temperature relies on comparing the damping with and without spin-cooling, using the relation $T_{\text{eff}} = T \frac{\gamma}{\gamma_{\text{eff}}}$ [7].

Modeling of the experiment For the most part of the paper, we model the experiment numerically using Monte-Carlo simulations that include the full three-level structure of the NV spin 1 system in the ground state (see Supplementary Material). For the spin-cooling and spin-spring effects shown in Fig. 2.c), the number of NV centers, polarization rate, Rabi frequencies, and angle between the NV centers and the main axis of the diamond are left as free parameters.

Experimental analysis of bistability and phonon-lasing The curve in Fig. 3-a)-i) shows the angular evolution of the particle as a function of the microwave detuning obtained using similar parameters than in the linear regime, but using a microwave and laser powers that fitted best the data in Fig.3-a)-ii) and a lower trapping frequency ($\omega_\phi/2\pi = 240$ Hz). Fig.3-a)-iii) shows the evolution of the librational mode angle as a function of time in this regime. Several of such curves were obtained for different microwave detunings, and are shown in the extended data. A Monte-Carlo simulation was also performed using our experimental parameters, with a microwave tuned to the red side, and shows similar jumps between the two stable points A and B. The data shown in Fig. 3-b)-i) of the main text show the evolution of power spectra for different microwave signal powers, when it is tuned to the blue of the ODMR transition. The onset of instability is seen at approximately 0 dBm. For a quantitative estimate of the threshold, we compute the area below the librational peak as a function of microwave detuning. This is shown in Fig. 3-b)-ii). Note that here the sensitivity of the power spectra to the angle may induce some systematic errors. For these measurements,

we fitted the data by the numerical model, and found good agreement with the numerical analysis, but a quantitative comparison with the experiment is difficult due to the above mentioned angle dependent sensitivity.

[1] T. Delord, P. Huillery, L. Schwab, L. Nicolas, L. Lecordier, and G. Hétet, "Ramsey interferences and spin echoes from electron spins inside a levitating macroscopic particle," Phys. Rev. Lett. **121**, 053602 (2018).

[2] T. Delord, L. Nicolas, M. Bodini, and G. Hétet, "Diamonds levitating in a paul trap under vacuum: Measurements of laser-induced heating via nv center thermometry," Applied Physics Letters **111**, 013101 (2017).

[3] Tom Delord, Louis Nicolas, Lucien Schwab, and Gabriel Hétet, "Electron spin resonance from nv centers in diamonds levitating in an ion trap," New Journal of Physics **19**, 033031 (2017).

[4] J.-P. Tetienne, L. Rondin, P. Spinicelli, M. Chipaux, T. Debuisschert, J.-F. Roch, and V. Jacques, "Magnetic-field-dependent photodynamics of single NV defects in diamond: an application to qualitative all-optical magnetic imaging," **14**, 103033 (2012).

[5] Erik Hebestreit, René Reimann, Martin Frimmer, and Lukas Novotny, "Measuring the internal temperature of a levitated nanoparticle in high vacuum," Phys. Rev. A **97**, 043803 (2018).

[6] J Millen, T Deesuwan, P Barker, and Janet Anders, "Nanoscale temperature measurements using non-equilibrium brownian dynamics of a levitated nanosphere," Nature nanotechnology **9**, 425 (2014).

[7] O. Arcizet, P. F. Cohadon, T. Briant, M. Pinard, and A. Heidmann, "Radiation-pressure cooling and optomechanical instability of a micromirror," Nature **444**, 71 EP – (2006).

Data availability statement The data that support the findings of this study are available from the corresponding author upon reasonable request.

Author Information Reprints and permissions information is available at www.nature.com/reprints. The authors declare no competing financial interests. Readers are welcome to comment on the online version of the paper. Publisher's note: Springer Nature remains neutral with regard to jurisdictional claims in published maps and institutional affiliations. Correspondence and requests for materials should be addressed to G. H.(gabriel.hetet@ens.fr).

The authors declare no competing interests.

EXTENDED DATA – CAPTIONS

D. Figure 1

Parametric spin-excitation of the librational mode a) Detection principle of the librational modes using microwave parametric excitation (top). Reflected light field amplitude as a function of time for one low librational mode frequency (170 Hz) at 1 mbar (below). b) Spin-mechanical resonance for two different microwave powers i) -20 dBm and ii) -10 dBm. c) Reflected light field amplitude as a function of time, for three microwave frequencies $2.617, 2.623$ and 2.634 GHz. Plain line shows a very good fit to the data (see Methods) using two sinus at the frequency of the parametrically excited librational mode (480 Hz) and of the closest librational mode (590 Hz) with an amplitude that is 30 times smaller.

E. Figure 2

Numerical simulations in the non-linear regime. a) Effective damping and spring constants as a function of the microwave detuning deduced by a numerical fit to the ring down curves (see Methods). Trace i), ii), iii), and iv) correspond to the increasing microwave Rabi frequencies $\Omega/2\pi = 50, 150, 200, 250$ kHz respectively. b) Evolution of the angle as a function of time after turning on a microwave to the blue of the spin resonance at a time $t = 20$ ms, showing amplification and finally lasing at $t = 120$ ms. c) Librational mode velocity as a function of microwave Rabi frequency, for three different values of the spin-lattice relaxation rate $1/T_1 = 1, 2$ and 3 kHz for trace i)-ii) and iii) respectively.

F. Figure 3

Numerical simulations of phonon-lasing Particle angle as a function of time upon sudden switching of a microwave signal on at a time t=0.02 s on the blue of the spin transition. The microwave power is above threshold so lasing can be observed. This curve was used to plot the histogram of Fig. 3-c) in the main text.

G. Figure 4

Calibration of sensitivity using NV magnetometry a) Upper panel: mechanically detected spin resonance for 3 different microwave powers. The dashed line is the locus of the signal minima. Lower panel: angle between the NV axis and magnetic field direction versus NV spin transition frequency. b) Optical signal as a function of time. c) Left panel : Sketch depicting the angular motion of the diamond upon magnetization of one class of NV spins using only two angles θ_x and θ_y for simplicity. B is the orientation of the magnetic field. Right panel : angular trajectory represented in the (θ_x, θ_y) space. We note O the particle orientation without NV magnetization ($M_z = 0$). The red/green line are the trajectories in the isotropic/anisotropic case respectively (see Methods). θ_d is the detected angle. d) Power spectrum of the Brownian motion for two different speckle alignments taken with a resolution bandwidth of 1 Hz. The red curves show all three librational modes. In blue, the detection is tuned to be mainly sensitive to the mode with the highest confinement frequency. The latter detection tuning is used for the data shown in a) and b).

H. Figure 5

Measurement of spin polarisation rates a) Sequences employed to measure the laser induced polarization rate to the ground state (trace i)) and to measure the polarization rate to the magnetic state $m_s' = -1$ *via* the microwave (trace ii)). The laser is kept on at all times for both sequences. b) Trace i) shows the PL rate at a time τ after having turned off the microwave signal. An exponential fit to the data gives a laser polarization time of 300 μs. Trace ii) shows the PL rate a time τ after having turned on the microwave signal. The polarization time to the magnetic state is here 124 μs.

I. Figure 6

Particle angle dynamics for different microwave detunings in the bistable regime Experimental observation of the particle angle as a function of time for the microwave frequencies : 2.8000, 2.8010, 2.8020, 2.8030, 2.8035, 2.8040 GHz, from trace a) to f), tuned to the red of the ESR transition. A histogram is shown on the right of each time-trace, showing the number of counts within each bin.

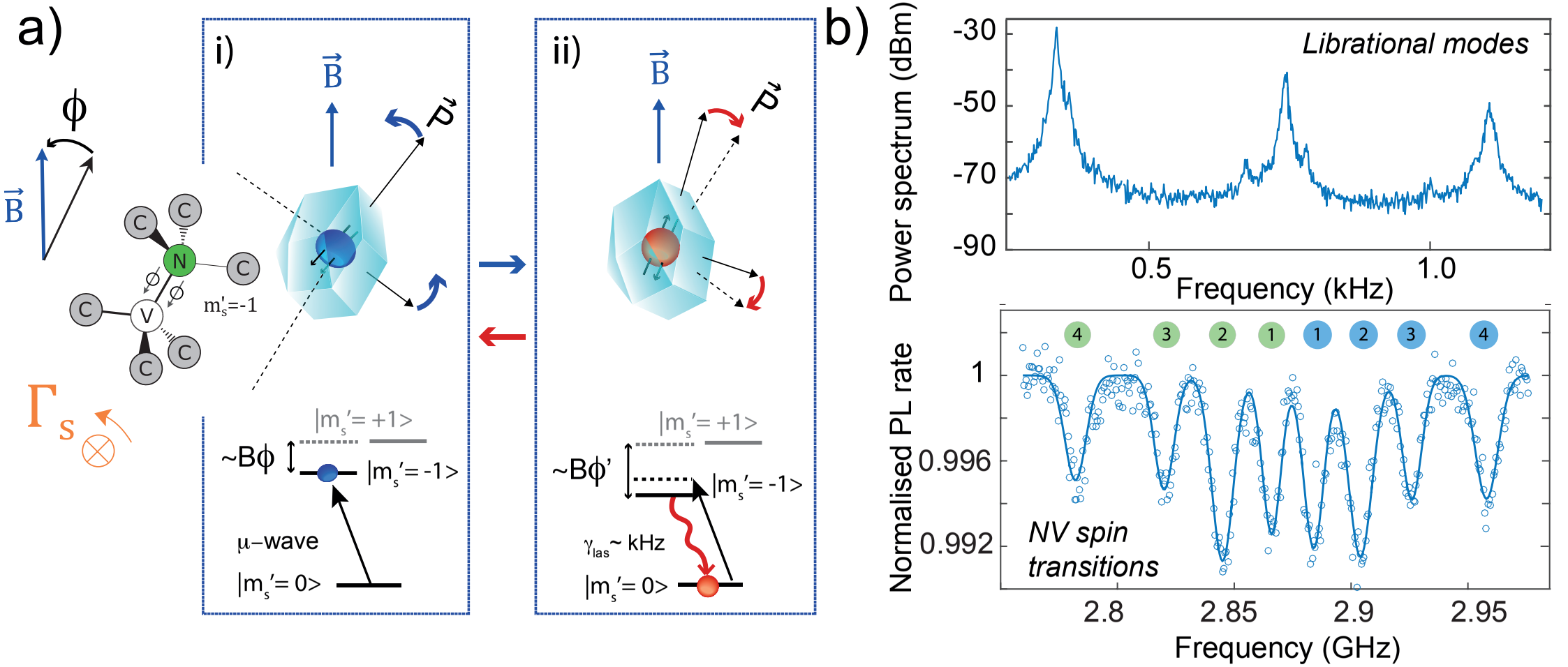
a)
i)
ii)
$\vec{B}$
ϕ
$\vec{p}$
C
N
V
m_s'=-1
Γ_s
$|m_s'= +1>$
$|m_s'= -1>$
$|m_s'= 0>$
~Bϕ
~Bϕ'
μ–wave
γ_{las} ~ kHz
b)
Librational modes
Power spectrum (dBm)
-30
-50
-70
-90
0.5
1.0
Frequency (kHz)
Normalised PL rate
1
0.996
0.992
4
3
2
1
1
2
3
4
NV spin transitions
2.8
2.85
2.9
2.95
Frequency (GHz)

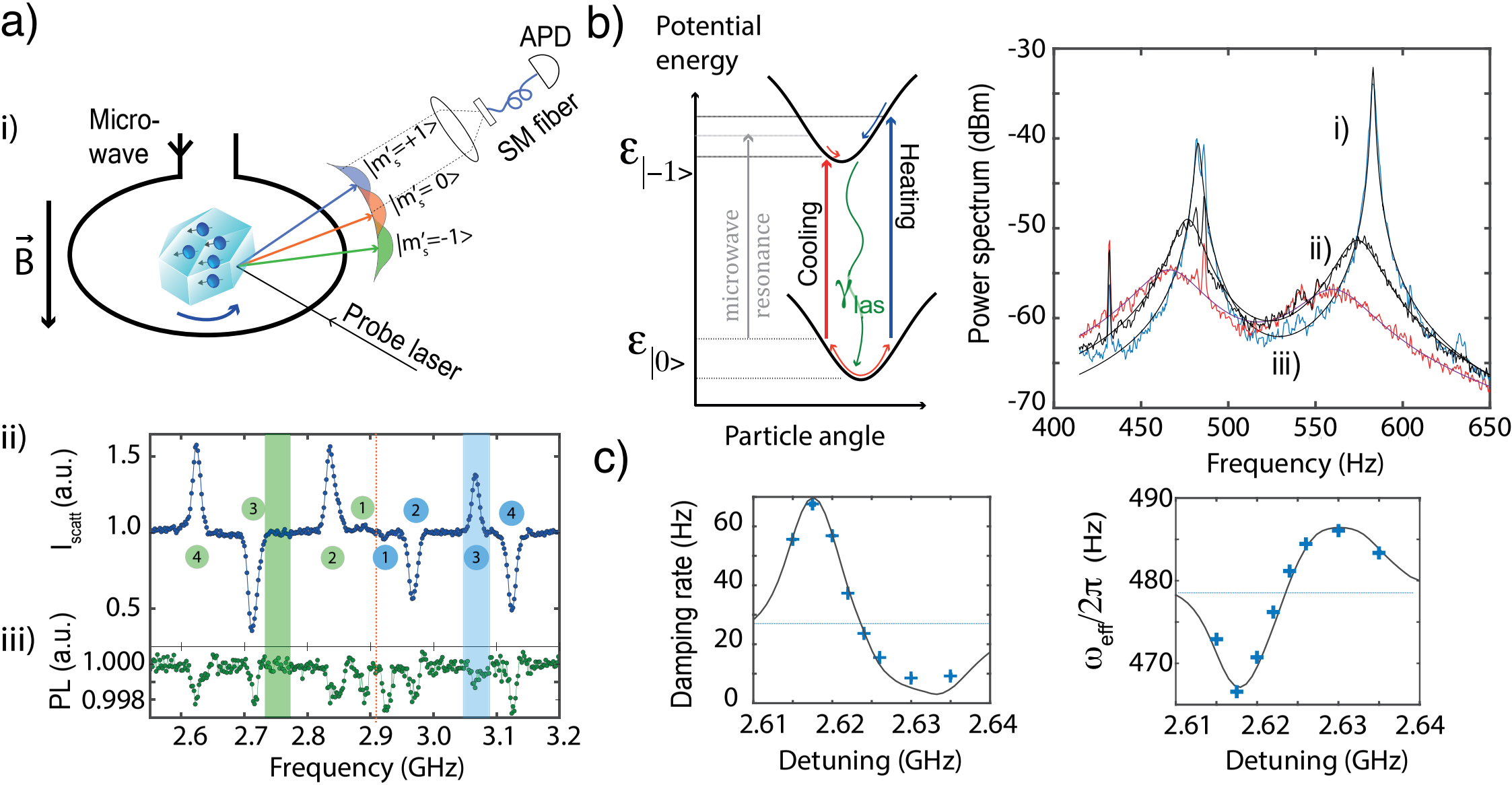
a)
i)
Micro-
wave
B
APD
SM fiber
|m's=+1>
|m's= 0>
|m's=-1>
Probe laser
ii)
iii)
I_scatt (a.u.)
PL (a.u.)
Frequency (GHz)
b)
Potential
energy
ε |−1>
ε |0>
microwave
resonance
Cooling
γ las
Heating
Particle angle
Power spectrum (dBm)
i)
ii)
iii)
Frequency (Hz)
c)
Damping rate (Hz)
Detuning (GHz)
ω eff/2π (Hz)
Detuning (GHz)

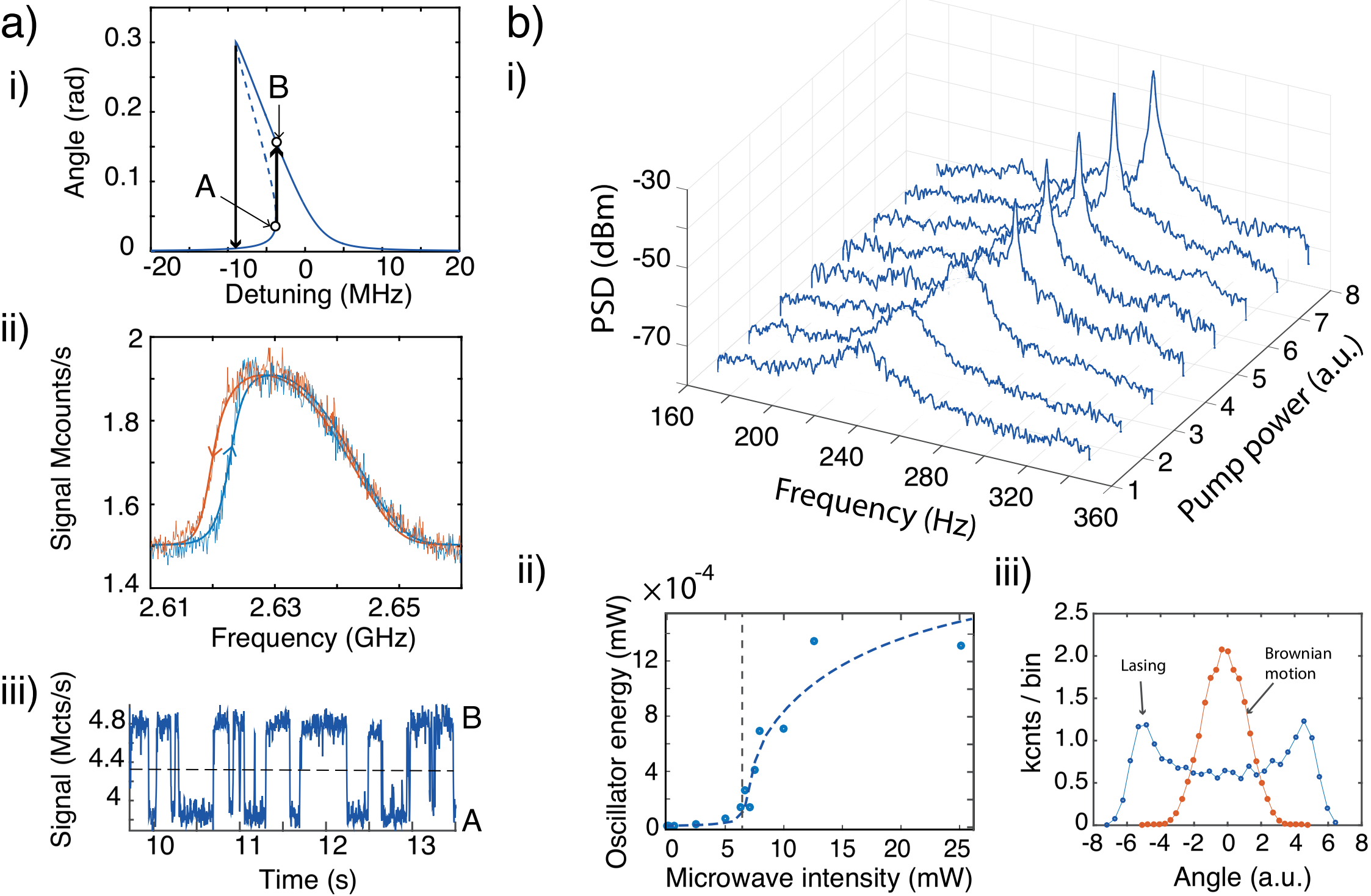
a)
i)
Angle (rad)
0.3
0.2
0.1
0
A
B
-20
-10
0
10
20
Detuning (MHz)
ii)
Signal Mcounts/s
2
1.8
1.6
1.4
2.61
2.63
2.65
Frequency (GHz)
iii)
Signal (Mcts/s)
4.8
4.4
4
B
A
10
11
12
13
Time (s)
b)
i)
PSD (dBm)
-30
-50
-70
160
200
240
280
320
360
Frequency (Hz)
1
2
3
4
5
6
7
8
Pump power (a.u.)
ii)
×10-4
Oscillator energy (mW)
12
8
4
0
0
5
10
15
20
25
Microwave intensity (mW)
iii)
kcnts / bin
2.5
2.0
1.5
1.0
0.5
0
Lasing
Brownian motion
-8
-6
-4
-2
0
2
4
6
8
Angle (a.u.)